Flat-top surface plasmon-polariton modes guided by double-electrode structures

Jaewoong Yoon[1], Seok Ho Song[1*], and Suntak Park[2]

[1]*BK21 Center in Department of Physics, Hanyang University, Seoul 133-791, Republic of Korea*
[2]*Basic Research Lab. Electronics and Telecommunications Research Institute, Daejon 305-700, Republic of Korea*
**Corresponding author: shsong@hanyang.ac.kr*
http://optics.hanyang.ac.kr

Abstract: We characterize the frequency dependence of symmetrically-coupled long-range surface plasmon-polaritons (sc-LRSPPs) excited on double-electrode slab waveguides composed of five layers of insulator(*I*) and metal(*M*) stacked in order of *IMIMI*. When the core insulator has a refractive-index larger than the cladding ones, there is no cut-off core-thickness(*D*) for sc-LRSPP modes in all frequency range likely for modes in a conventional dielectric slab waveguide. At a specific frequency of ω_c which depends on the index difference of insulator layers and the thickness of metal, the sc-LRSPP modes are non-dispersive at all for change in *D*. Furthermore, regardless of *D* alteration, the modes at $\omega = \omega_c$ consistently maintain a perfect flat-top profile in the core region and identical decay tails in the cladding. The sc-LRSPP modes with these prominent characteristics may excite an active medium sandwiched in between the metal layers very uniformly, therefore it will be interesting to implement such a non-dispersive flat-top mode for nonlinear applications of SPP waveguides.

OCIS codes: (130.2790) Guided waves, (250.5403) Plasmonics

References and links

1. H. Raether, *Surface plasmons on Smooth and Rough Surfaces and on Gratings*, (Springer-Verlag, Berlin, 1988).
2. W. L. Barnes, A. Dereux, and T. W. Ebbesen, (Insight review articles) "Surface plasmon subwavelength optics," Nature **424**, 824-830 (2003).
3. R. W. Wood, "On a remarkable case of uneven distribution of light in a diffraction grating spectrum," Phil. Mag. **4**, 396 (1902).
4. R. W. Wood, "Anomalous diffraction gratings," Phys. Rev. **48**, 928-936 (1935).
5. U. Fano, "The theory of anomalous diffraction gratings and of quasi-stationary waves on metallic surfaces (Sommerfeld's waves)," J. Opt. Soc. Am. **31**, 213-222 (1941).
6. S. Linden, J. Kuhl, and H. Giessen, "Controlling the interaction between light and gold nano particles: Selective suppression of extinction," Phys. Rev. Lett. **86**, 4688 (2001).
7. E. Kretchmann and H. Raether, "Radiative decay of nonradiative surface plasmons excited by light," Z. Naturkorsch. A **23**, 2135-2136 (1968).
8. A. Otto, "Excitation of nonradiative surface plasma waves in silver by the method of frustrated total reflection," Z. Phys. **216**, 398 (1968).
9. J. Homola, S. S. Yee, and G. Gauglitz, "Surface plasmon resonance sensors: review," Sensors Actuat. B **54**, 3-15 (1999).
10. E. Ozbay, (Review) "Plasmonics: Merging photonics and electronics at nanoscale dimensions," Science **311**, 189-193 (2006).
11. S. A. Maier, P. G. Kik, H. A. Atwater, S. Meltser, E. Harel, B. E. Koel, and A. A. G. Requicha, "Local detection of electromagnetic energy transport below the diffraction limit in metal nanoparticle plasmon waveguides," Nat. Mater. **2**, 229-232 (2003).
12. M. I. Stockman, "Nanofocusing of optical energy in tapered plasmonic waveguides," Phys. Rev. Lett. **93**, Art. No. 137404 (2004).
13. J. R. Krenn and J.-C. Weeber, "Surface plasmon polaritons in metal stripes and wires," Phil. Trans. R. Soc. Lond. A **362**, 739-756 (2004).

#89161 - $15.00 USD Received 29 Oct 2007; revised 29 Nov 2007; accepted 29 Nov 2007; published 7 Dec 2007

14. D. Sarid, "Long-range surface-plasma waves on very thin metal films," Phys, Rev. Lett. **47**, 1927-1930 (1981).
15. P. Berini, "Plasmon-polariton waves guided by thin lossy metal films of finite width: Bounded modes of symmetric structures," Phys. Rev. B **61**, 10484 (2000).
16. T. Nikolajsen, K. Leosson, I. Salakhutdinov, and S. I. Bozhevolnyi, "Polymer-based surface-plasmon-polariton stripe waveguides at telecommunication wavelengths," Appl. Phys. Lett. **82**, 668-670 (2003).
17. P. Berini, R. Charbonneau, N. Lahoud, and G. Mattiussi, "Characterization of long-range surface-plasmon-polariton waveguides," J. Appl. Phys. **98**, Art. No. 043109 (2005).
18. T. Nikolajsen, K. Leosson, S. I. Bozhevolnyi, "In-line extinction modulator based on long-range surface plasmon polaritons," Opt. Commun. **244**, 455-459 (2005).
19. S. Park and S. H. Song, "Polymeric optical attenuator based on long range surface plasmon polaritons," Electron. Lett. **42**, 402-404 (2006).
20. G. Gagnon, N. Lahoud, G. A. Mattiussi, and P. Berini, "Thermally activated variable attenuation of long-range surface plasmon-polariton waves," J. Lightwave Technol. **24**, 4391-4402 (2006).
21. A. Boltasseva, T. Nikolajsen, K. Leosson, K. Kjaer, M. S. Larsen, and S. I. Bozhevolnyi, "Integrated optical components utilizing long-range surface plasmon polaritons," J. Lightwave technol. **23**, 413-422 (2005).
22. H. S. Won, K. C. Kim, S. H. Song, C.-H. Oh, P. S. Kim, S. Park, and S. I. Kim, "Vertical coupling of long-range surface plasmon polaritons," Appl. Phys. Lett. **88**, Art. No. 011110 (2006).
23. R. Charbonneau, C. Scales, I. Breukelaar, S. Fafard, N. Lahoud, G. Mattiussi, and P. Berini, "Passive integrated optics elements based on long-range surface plasmon polaritons," J. Lightwave Technol. **24**, 477-494 (2006).
24. A. Boltasseva, S. I. Bozhevolnyi, T. Søndergaard, T. Nikolajsen, and K. Leosson, "Compact Z-add-drop wavelength filters for long-range surface plasmon polaritons," Opt. Express **13**, 4237-4243 (2005).
25. S. J. Charbonneau, R. Charbonneau, N. Lahoud, G. A. Mattuissi, and P. Berini, "Bragg gratings based on long-range surface plasmon-polariton waveguides: Comparison of theory and experiment," IEEE J. Quantum Electron. **41**, 1480-1491 (2005).
26. G. I. Stegeman and J. J. Burke, "Long-range surface-plasmons in electrode structures," Appl. Phys. Lett. **43**, 221-223 (1983).
27. E. N. Economou, "Surface plasmons in thin films," Phys. Rev. **182**, 539-554 (1969).
28. E. D. Palik, *Handbook of Optical Constants of Solids II*, (Academic Press, San Diego, 1998).
29. M. I. Stockman, "Nanofocusing of optical energy in tapered plasmonic waveguides," Phys. Rev. Lett. **93**, Art. No. 137404 (2004).
30. U. Schröter and A. Dereux, "Surface plasmon polaritons on metal cylinders with dielectric core," Phys. Rev. B **64**, Art. No. 125420 (2001).

1. **Introduction**

Surface plasmon-polaritons (SPPs) are surface localized waves propagating on an interface between a metal and a dielectric. Over a frequency band in which the dielectric constant of metal is less than minus of that of adjacent dielectric, SPPs are excited by coupling between collective oscillations of free electrons and evanescent electromagnetic (EM) waves [1,2]. This resonant coupling gives SPPs the peculiar properties of surface localizations and field enhancements, which make a lightwave be able to interact strongly with nanoscopic structures by mediating them. For these natures, SPPs have been widely studied since the first optical observation in the anomalous diffraction from a metallic grating by Wood [3,4] and its causal explanation by Fano [5]. Applications of SPPs are ranging from colored glasses [6] or attenuated total reflection (ATR) based devices [7-9] to even potentials for merging photonic and electronic integrated circuits recently [2,10-13].

One of the active fields regarding SPPs is applications of long-range SPPs (LRSPPs). LRSPPs are supported by anti-symmetric charge coupling of SPPs on two surfaces of a thin metal film of which thickness is comparable to or less than the penetration depth of EM wave. For its small propagation constant and nearly transversal field components, internal loss (mainly ohmic loss in the metal) is small and direct end-fire coupling with any fundamental mode of a conventional dielectric based waveguide is very efficient [1,14,15]. Though LRSPPs are not so confined modes and the loss is still larger than dielectric waveguides, high cladding sensitivity and parallelism of optical and electrical signals make them useful for integrated optical devices. In addition, LRSPP waveguides consisting of about 20 *nm* thick and a few μm wide metal strips are much easier to be fabricated by conventional lithography

#89161 - $15.00 USD Received 29 Oct 2007; revised 29 Nov 2007; accepted 29 Nov 2007; published 7 Dec 2007

technique than index-guiding dielectric waveguides which require a wavelength scale depth in index steps. Many integrated passive and active optical devices based on LRSPPs such as channel waveguides [16,17], thermo-optic modulators [18-20], directional couplers [21-23], and Bragg grating filters [24,25] were reported recently in this context.

A double-electrode structure which consists of two metallic thin film had been reported as a possible waveguide structure supporting LRSPPs quite long time ago [26]. Stegeman *et al* pointed out that LRSPPs on a double-electrode waveguide can be controlled more actively by using electro- or acousto-optic materials as a central dielectric medium because the pair of the metal film itself offers to supply DC electric field in the core dielectric medium. This structure has some other advantages over single-film LRSPP waveguides. As any homogeneous change in the core dielectric material does not break vertical symmetry of the structure, LRSPPs exist over much broader range of index contrast between the core and the cladding dielectric [26]. Therefore, the structure does not require a nearly free standing metal film for LRSPP based fluidic sensors, and it can include dielectric grating or photonic crystal structures in the core dielectric medium. In spite of those advantages, little attention has been paid to a double-electrode LRSPP waveguide. Dispersion relations and attenuation properties of LRSPPs excited on a double-electrode waveguide had been reported [26, 27], but decisive questions for its practical applicability considering dependence of propagation lengths and field identities on operation frequency have not been addressed so far.

In this paper, we study frequency dispersive characteristics of LRSPPs on double-electrode waveguides. Dispersion curves and corresponding field identities of the modes are analyzed according to the structural parameters of core and cladding dielectrics. The analysis allows us to describe double-electrode LRSPPs in a general manner with the help of definition of a characteristic frequency by which different core-thickness dependencies are classified. Several interesting properties such as cut-off core-thickness at the vicinity of which the attenuation is largely reduced without any need of thinning metallic films, transiently saturated attenuation which can be used as a switching operation point, and the thickness-dispersionless flat-top LRSPP which can provide efficient adiabatic mode scaling are discussed on this basis. In section 2, dispersion relation of double-electrode waveguide structures is briefly derived. Dispersion curves in terms of frequency and effective-index of LRSPP modes are presented in Section 3, where dependence of the dispersion relation on the core-thickness is discussed for both low-index-core and high-index-core structures. The characteristic frequency that offers a criterion classifying the characteristic groups of LRSPP modes is described in Section 4. Field identities and attenuation properties at relative frequencies to ω_c are investigated in Section 5. Finally we conclude our analysis on double-electrode waveguide structures in Section 6.

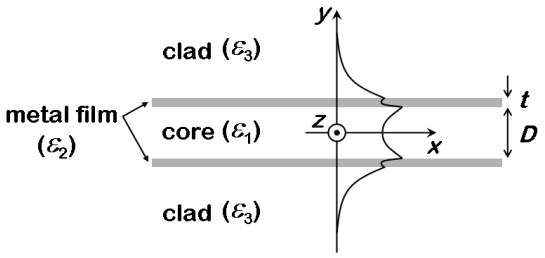

Fig. 1. Schematic of a double-electrode slab waveguide structure and the shape of magnetic field profile for a symmetrically coupled LRSPP.

#89161 - $15.00 USD Received 29 Oct 2007; revised 29 Nov 2007; accepted 29 Nov 2007; published 7 Dec 2007

2. Dispersion relation of double-electrode waveguides

A double-electrode waveguide considered here is illustrated in Fig. 1. It consists of two identical metal slabs with a dielectric constant ε_2 surrounded by core (ε_1) and cladding (ε_3) dielectrics. Thickness of the core dielectric and the metal film is D and t, respectively. In frequency domain, the magnetic field of a transverse magnetic (TM) polarized mode with propagation constant β in this structure can be written in general as

$$\mathbf{H} = H_0 f(y) \exp(i\beta x)\mathbf{e}_z, \tag{1}$$

where

$$f(y) = \begin{cases} \cosh(\alpha_1 y) \ \ or \ \ \sinh(\alpha_1 y) & (0 \le y \le D/2) \\ A\exp(\alpha_2[y - D/2]) + B\exp(-\alpha_2[y - D/2]) & (D/2 \le y \le t + D/2) \\ C\exp(-\alpha_3[y - D/2 - t]) & (t + D/2 \le y) \end{cases} \tag{2}$$

in the region $y \ge 0$. The $\cosh(\alpha_1 y)$ or $\sinh(\alpha_1 y)$ is taken for a symmetric or an anti-symmetric mode respectively. The field in the region $y \le 0$ is also provided by continuation of Eq. (2), and the electric field is given by $\mathbf{E} = -\nabla \times \mathbf{H}/(i\omega\varepsilon_m)$ for m = 1, 2, or 3. The decay constant in each layer is given by

$$\alpha_m = (\beta^2 - \varepsilon_m k_0^{\,2})^{1/2}, \ \ m = 1, \ 2, \text{ or } 3. \tag{3}$$

Requiring continuity of the tangential fields (H_z and E_x) at the interfaces leads to a dispersion relation and the amplitudes of a symmetric mode, A, B, and C in Eq. (2), as follows.

$$\frac{\alpha_2\alpha_3}{\varepsilon_2\varepsilon_3} + \frac{\alpha_1\alpha_2}{\varepsilon_1\varepsilon_2}\tanh(\alpha_1 D/2) + \left(\frac{\alpha_2}{\varepsilon_2}\right)^2 \tanh(\alpha_2 t) + \frac{\alpha_3\alpha_1}{\varepsilon_3\varepsilon_1}\tanh(\alpha_1 D/2)\tanh(\alpha_2 t) = 0 \tag{4}$$

$$\begin{cases} A = \dfrac{1}{2}\left[\cosh(\alpha_1 D/2) + \dfrac{\alpha_1/\varepsilon_1}{\alpha_2/\varepsilon_2}\sinh(\alpha_1 D/2)\right] \\ B = \dfrac{1}{2}\left[\cosh(\alpha_1 D/2) - \dfrac{\alpha_1/\varepsilon_1}{\alpha_2/\varepsilon_2}\sinh(\alpha_1 D/2)\right] \\ C = \left[\cosh(\alpha_1 D/2)\cosh(\alpha_2 t) + \dfrac{\alpha_1/\varepsilon_1}{\alpha_2/\varepsilon_2}\sinh(\alpha_1 D/2)\sinh(\alpha_2 t)\right] \end{cases} \tag{5}$$

Expressions for an anti-symmetric mode can be obtained by exchanging cosh and sinh to each other. The dispersion relation in Eq. (4) gives a complex propagation constant of $\beta = \beta_r + i\beta_i$. Frequency dependent characteristics of β_r provide a dispersion curve according to D, and $1/(2\beta_i)$ defines propagation length where the mode intensity is decayed down to its $1/e$ value after propagation.

It is known that four modal solutions exist implicitly in Eq. (4) as SPP modes for a double-electrode structure [26,27]. Each of them represents a combination out of symmetrically or anti-symmetrically coupled (sc- or ac-) long-range SPPs (LRSPPs) or short-range SPPs (SRSPPs). Internal loss is smaller in long-range SPP modes while larger in short-range SPP

#89161 - $15.00 USD Received 29 Oct 2007; revised 29 Nov 2007; accepted 29 Nov 2007; published 7 Dec 2007

modes since they possess a node in the metal slabs. Each of the long-range and short-range SPPs splits again into two separate modes according to their symmetry referenced at the center of the core dielectric. Only a symmetrically-coupled long-range SPP, sc-LRSPP, mode whose magnetic field has a profile depicted schematically in Fig. 1 will be considered hereafter, because an anti-symmetrically coupled long-range SPP may hardly be excited by direct end-fire coupling and even disappears when the core thickness is less than about the decay length of SPPs excited on a single-electrode waveguide [26].

Complex β which satisfies Eq. (4) is found by 2 stage processes. On the first stage, an approximate solution is given by observing values of left-hand side of Eq. (4). Reciprocals of absolute square values of the left-hand side of Eq. (4) are evaluated along real β-axis within a specified domain of β. A range $\varepsilon_3^{1/2}k_0 < \beta < 2\varepsilon_3^{1/2}k_0$ was enough to completely contain the sc-LRSPP dispersion curve for an arbitrary core thickness over a frequency domain from DC to visible light. The reciprocal of absolute square value of the equation shows series Lorentzian-shaped peaks centered at $\mathrm{Re}\{\beta_{\text{sc-LRSPP}}\}$ and $\mathrm{Re}\{\beta_{\text{sc-SRSPP}}\}$. The peak center position (β_0) closest to $\varepsilon_3^{1/2}k_0$ among them is recognized as an initial guess for β_r of the sc-LRSPP. Its full-width at half-maximum ($\Delta\beta$) is assigned as an approximate value of $2\beta_i$. On the second stage, Newton method starting at $\beta^{(0)} = \beta_0 + i\Delta\beta/2$ is applied to find the exact complex β for the sc-LRSPP until the propagation constant converges within $|\beta^{(n+1)} - \beta^{(n)}|/k_0 = \pm 1.1\times10^{-16}$ during consecutive iterations. As β_i/β_r is an order of 10^{-3} or less (β is dominantly real), the first stage gives a well defined initial guess and provides a good repeatability in finding roots.

3. Symmetrically-coupled long-range surface plasmon-polaritons

Two different cases of low-index-core and high-index-core structures are analyzed to find out global features of sc-LRSPPs. Let's specify, for simplicity, the metal slabs by a 20 *nm*-thick gold film and the refractive index of the core (cladding) dielectric by 1.45 (1.47) for the low-index-core structure and by 1.47 (1.45) for the high-index-core structure, as shown in the insets of Fig. 2. Dispersion curves calculated by Eq. (4) are shown in Fig. 2 for the two core structures. The effective index of a sc-LRSPP mode is defined as a relative propagation constant of $n_{eff}=\beta_r/k_0$, and the frequency is normalized by the frequency of an electromagnetic wave whose vacuum wavelength is 1 μm. A Drude model fitted to give ε_2 = -118+11.58*i* at 1550 *nm* vacuum wavelength is used for the frequency dependent dielectric constant of Au [28].

Figures 2(a) and 2(b) show frequency dispersive characteristics of the effective indices for the sc-LRSPP modes exited at the two double-electrode waveguide structures with low-index-core and high-index-core, respectively. The dispersion curves exist only in the shadow regions as D increases from 0 μm to infinity, and those depicted in between the two asymptotic limits are of the finite core-thickness ranging from 0.2 μm to 6.0 μm in 0.2 μm steps. It is worth discussing first the two limits of no core dielectric (D = 0 μm) and infinitely thick core dielectric ($D\rightarrow\infty$). The dispersion curves and modal properties for any other finite cores will be addressed in between these two limits as shown in Fig. 2. For the limit case when D = 0 μm, the dispersion curves exist over the continuous range starting from the zero frequency for both core-index structures. This no-core limit is the same as the dispersion of LRSPP modes for a single-electrode waveguide with a metal thickness of 2t (40 *nm*). On the other hand, the dispersion curves when $D\rightarrow\infty$ have a characteristic frequency ω_c at the point of 1.47 effective index. In the frequency range smaller than ω_c there is no LRSPP mode for the infinite core thickness. Since when $D\rightarrow\infty$ there is no coupling between the modes on the two metal waveguides, the dispersion curves shown above the ω_c are the same as the dispersion of a asymmetric single-electrode waveguide composed by a metal film with thickness of t (20 *nm*) and two different surrounding dielectrics with n =1.45 and n =1.47. In the case of the 20 *nm*-

#89161 - $15.00 USD Received 29 Oct 2007; revised 29 Nov 2007; accepted 29 Nov 2007; published 7 Dec 2007

thick Au film sandwiched by two dielectrics with the refractive indices of 1.45 and 1.47, ω_c is $1.09 \times 2\pi c/\mu m$ and the corresponding vacuum wavelength is 917.08 *nm*.

For a finite core-thickness in the low-index-core structure shown in Fig. 2(a), there is no low frequency cut-off in the dispersion curve as D increases up to 1.0 μm. For a core-thickness larger than 1.0 μm, on the other hand, low-frequency cut-off appears and it approaches ω_c as D increases. Therefore the core-thickness dependent characteristics of sc-LRSPP modes is quite different according to the relative position of the frequency to ω_c. For a fixed frequency lower than ω_c, as D gets larger, the effective index decreases down to the cladding index of n_3 (1.47) as D approaches a particular value, $D_{cut\text{-}off}$, and the sc-LRSPP modes disappear when $D > D_{cut\text{-}off}$. That is, there is a range of the core thickness that supports sc-LRSPPs when $\omega < \omega_c$. This behavior of the effective index is shown in Fig 2(c). Dashed and dash-dotted line represents D-dependent effective index at two different frequencies below ω_c. Corresponding vacuum wavelength is 1550(ω_1) and 1100(ω_2) *nm*, respectively. Please note that grey lines below 1.47 indicate not true solution but initial guesses given by peak positions of reciprocal value of the dispersion equation. There is no β satisfying Eq. (4) below effective index of 1.47. It is confirmed that the effective index decreases for increasing D and finally disappear for $D > D_{cut\text{-}off}$. $D_{cut\text{-}off}$ is 1.340 μm for ω_1 and 1.688 μm for ω_2. For a core thickness just below $D_{cut\text{-}off}$, the mode size diverges to infinity since the decay constant in the cladding given by $\alpha_3=[\beta^2-n_3^2k_0^2]^{1/2}$ is about to vanish and therefore the decay length of the

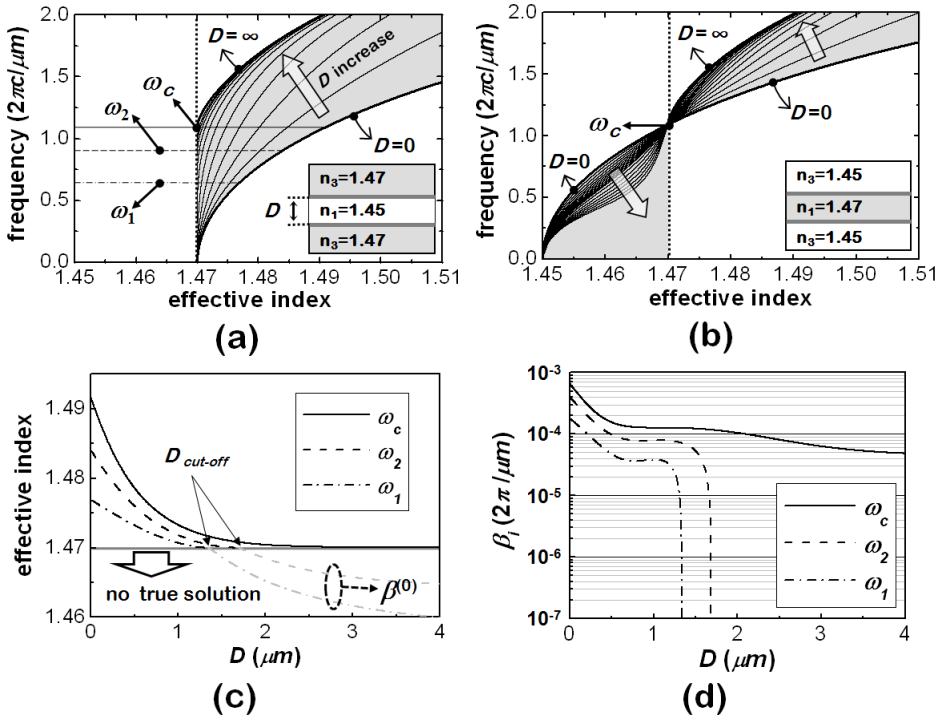

Fig. 2. The dispersion curves of sc-LRSPPs for two different cases of (a) low index core (n_1=1.45, n_3=1.47) and (b) high index core (n_1=1.47, n_3=1.45). Two asymptotic limits of D = 0 μm and $D = \infty$ are indicated by two thick curves on the boundaries of grey regions, and the dispersion curves in the grey region are of the core thicknesses ranging from 0.2 μm to 6.0 μm in 0.2 μm step. Please note that the core is thicker as the curve approaches the boundary of the grey region marked by '$D = \infty$'. (c) and (d) shows thickness dispersive characteristics of effective index and β_i for several frequencies below ω_c, respectively. Relative locations in the dispersion diagram for ω_1 and ω_2 are indicated by horizontal lines in (a).

#89161 - $15.00 USD Received 29 Oct 2007; revised 29 Nov 2007; accepted 29 Nov 2007; published 7 Dec 2007

evanescent tail (1/ α_3) stretched into the cladding diverges to infinity. The energy dissipated as ohmic loss in the metal will vanish too as shown in Fig 2(d). Therefore, it is expected that the propagation length will be largely extended just before the mode cut-off. $D_{cut\text{-}off}$ becomes larger for a higher frequency and infinite when $\omega = \omega_c$. For $\omega > \omega_c$ there is no cut-off core thickness and therefore no drastic extension in the propagation length is expected over the frequency range higher than ω_c.

On the other case of the high-index-core structure, frequency dependence of the sc-LRSPP modes is quite interesting as shown in Fig. 2(b). All curves are crossing at a single position at (n_1,ω_c) regardless of the value of D. When $\omega = \omega_c$ the propagation constant of sc-LRSPP mode is non-dispersive on D. Any cut-off core thickness does not exist over the full frequency range, so the internal loss of the sc-LRSPP modes never decreases extremely low. For $\omega < \omega_c$ the effective index has a value less than n_1 (1.47) and gradually approaches n_1 as D increases, while for $\omega > \omega_c$ dependence of the dispersion relation on D is similar to the low-index-core case. The sc-LRSPP mode with a larger core thickness reduces to a fundamental mode of dielectric slab waveguide which consists of the same core and cladding dielectrics without metal. A physical origin of existence of the crossing point at (n_1,ω_c) in the high-index-core structure can be clearly found by requiring Eq. (4) to be specified at the condition that $\beta = n_1 k_0$ and $\alpha_1 = 0$. Under this specific condition, the dispersion relation is reduced to $(\alpha_3/\varepsilon_3) + (\alpha_2/\varepsilon_2)$ $\tanh(\alpha_2 t) = 0$, and therefore it has no dependence on D. It can be deduced that eigen frequencies of the sc-LRSPP modes which have the effective index equal to the core index must keep in constant to be ω_c even for core-thickness variation.

Now we would like to summarize the frequency-dependent characteristics of sc-LRSPP modes excited on double-electrode structures as follows: In low-index-core case shown in Fig. 2(a), a cut-off core thickness exists for sc-LRSPP modes at a frequency range less than the characteristic frequency ω_c and mode size and propagation length become extremely extended just before the cut-off. For $\omega > \omega_c$, on the other hand, a sc-LRSPP mode can always be supported for arbitrary core thickness without a drastic extension of its mode size and propagation length. In low-index-core case shown in Fig. 2(b), when $\omega < \omega_c$ sc-LRSPP modes approach a fundamental mode of dielectric slab waveguide gradually from a single-electrode LRSPP mode as D increases. At $\omega = \omega_c$ the propagation constants of sc-LRSPP modes are non-dispersive and equal to $n_1 k_0$ even for core-thickness variation. For $\omega > \omega_c$, the frequency-dependent characteristics are the same as the low-index case.

4. The characteristic frequency

The characteristic frequency ω_c can be derived from the dispersion relation when propagation constant has no dependence on D, $(\alpha_3/\varepsilon_3) + (\alpha_2/\varepsilon_2) \tanh(\alpha_2 t) = 0$, as follow.

$$\omega_c = \frac{c}{t} \frac{1}{\left[\varepsilon_1 - \varepsilon_2(\omega_c)\right]^{1/2}} \tanh^{-1}\left(-\frac{\varepsilon_2(\omega_c)}{\varepsilon_3} \left[\frac{\varepsilon_1 - \varepsilon_3}{\varepsilon_1 - \varepsilon_2(\omega_c)} \right]^{1/2} \right) \qquad (6)$$

To extract the value of ω_c in terms of the three dielectric constants and the metal thickness is not straightforward, but it is plausible to estimate its dependence on the index contrast, $\Delta n = n_3 - n_1$, between the dielectric layers. If $\Delta n = 0$ (viz. $\varepsilon_1 - \varepsilon_3 = 0$), $\omega_c = 0$ obviously. For a non-zero or even a large Δn, intuitively ω_c can be estimated from the dispersion diagrams in Fig. 2(b). In fact, the reduced equation of $(\alpha_3/\varepsilon_3) + (\alpha_2/\varepsilon_2) \tanh(\alpha_2 t) = 0$ is exactly the same as the dispersion relation of LRSPPs excited on a single-electrode waveguide consisting of a single metal slab with thickness of $2t$ surrounded by dielectric with ε_3. ω_c is the frequency of the LRSPP mode on this single-electrode waveguide when the relation $\beta = n_1 k_0$ satisfied.

#89161 - $15.00 USD Received 29 Oct 2007; revised 29 Nov 2007; accepted 29 Nov 2007; published 7 Dec 2007

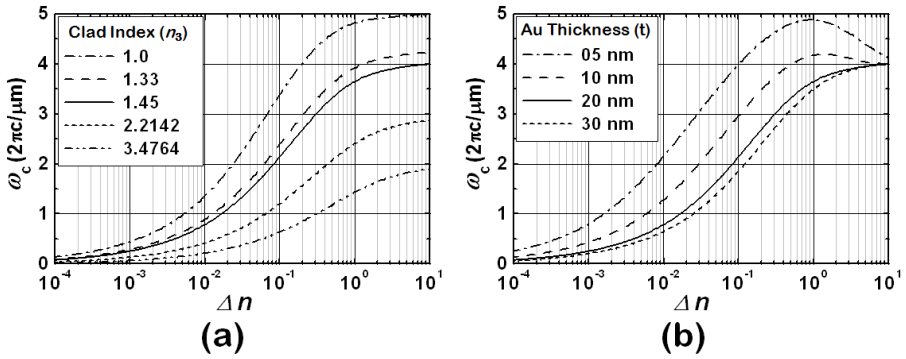

Fig. 3. Dependences of the characteristic frequency on the index difference for several refractive indices of the cladding (a) and some thicknesses of the metal slab (b). The Au thickness is fixed at 20 *nm* for (a), and the refractive index of the cladding is fixed at 1.45 for (b) respectively.

Therefore, for the structures considered in Fig. 2, ω_c is a point corresponding to the effective index of n_1. If n_1 increases, ω_c increases along the curve for D = 0 μm. For a large Δn, ω_c approaches a cut-off frequency of the single-electrode LRSPP, that is $\omega_c \rightarrow \omega_p/(1+\varepsilon_3)^{1/2}$.

Figure 3 shows dependence of ω_c on the index contrast Δn and the metal thickness t. In Fig. 3(a), the cladding index n_3 is chosen from some typical dielectric materials like silica (1.45), $LiNbO_3$ (2.2142), and silicon (3.4764) taken in the Ref. 40 by interpolating at λ_0 = 1550 *nm*, while the metal thickness is fixed at 20 *nm*. It can be confirmed that ω_c converges to $\omega_p/(1+\varepsilon_3)^{1/2}$ for a large index contrast. In the order of n_3 = 1.0, 1.33, 1.45, 2.2142, and 3.4764, the values of $\omega_p/(1+\varepsilon_3)^{1/2}$ normalized by $2\pi c/\mu m$ are 5.00, 4.25, 4.01, 2.91, and 1.95, respectively. In the same order of n_3, Δn that gives ω_c corresponding to the vacuum wavelength of 1550 *nm* is 2.14×10^{-3}, 5.09×10^{-3}, 6.62×10^{-3}, 2.44×10^{-2}, and 1.30×10^{-1}, respectively. For n_3 = 1.45, the ω_c dependence on the metal thickness is shown in Fig. 3(b). As Δn increases, ω_c converges to a constant value of 6.62×10^{-3} even for the different thickness, but ω_c grows more rapidly for a smaller t. It is confirmed that ω_c is tunable over broad spectrum from an optical communication to whole visible frequency range with acceptable index differences of $10^{-3} \sim 1$.

5. Propagation lengths and field profiles

Figures 4(a) and 5(a) show propagation length defined by $1/(2\beta_i)$ for sc-LRSPP modes excited on the two double-electrode structures with low-index core and high-index core, respectively. D varies from 0 μm to 8 μm. Three representative vacuum wavelengths (λ_0) of 667 *nm*, 917 *nm*, and 1550 *nm* are selected to compare the propagation lengths for three different frequency regions of $\omega < \omega_c$, $\omega = \omega_c$ (= 3.27×10^{14} *rad./s*), $\omega > \omega_c$, respectively. In case of low-index core shown in Fig. 4(a), frequency characteristics of sc-LRSPP propagation length dependent on D variation are clearly recognizable with the three black line curves. At λ_0 = 1550 *nm* ($\omega < \omega_c$, dashed black line), the propagation length increases exponentially for a small core thickness up to 0.7 μm before the transient saturation at the vicinity of 1 μm, and it gradually diverges without any supported sc-LRSPP mode after 1.33 μm. The behaviors of the exponential increase and the transient saturation are also seen at λ_0 = 917 *nm* ($\omega = \omega_c$, dash-dotted black line) bellow the 1.5 μm core-thickness. The two grey curves near the solid black line of 917 *nm* represent those for the frequencies adjacent to ω_c, for instance, ω_c - 0.17×10^6 *rad./s* for the upper grey and ω_c + 2.07×10^6 *rad./s* for the lower grey line. At λ_0 = 667 *nm* ($\omega > \omega_c$), on the other hand, the propagation length keep in constant for large D variations. It is noted that,

#89161 - $15.00 USD Received 29 Oct 2007; revised 29 Nov 2007; accepted 29 Nov 2007; published 7 Dec 2007

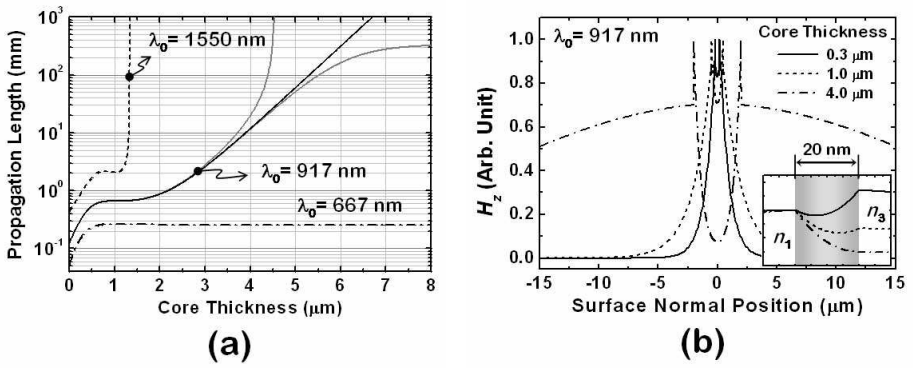

Fig. 4. (a). Dependences of the propagation lengths of sc-LRSPPs on the core thickness for the case of low index core at several wavelengths. The vacuum wavelengths are selected as representatives for $\omega<\omega_c$ (dashed line), $\omega=\omega_c$ (black solid line) and $\omega>\omega_c$ (dash-dotted line). Each of the upper and the lower grey solid curve represents just below and over the characteristic frequency respectively, and the corresponding differences from ω_c are -0.17 and $+2.07\times10^6$ *rad./s*. (b) Field profiles (H_z) of a sc-LRSPP at $\omega=\omega_c$ for the case of low index core. The inset shows the profiles normalized by its value at the core-metal interface in the metal film. In the inset, grey region indicates the metal film.

at $\omega = \omega_c$, the propagation length does not go to infinity abruptly after the transient saturation but increases exponentially and that the propagation behavior suffers from a sudden divergence or a bound limit even for a small amount of frequency deviation from ω_c.

A reason exhibiting the transient saturation near the core thickness of about wavelength scale can be found from transition property of the mode profiles as D varies. Figure 4(b) shows the normalized H_z components of sc-LRSPP modes when D = 0.3, 1.0, and 4.0 μm, where the surface normal position at 0 μm means the center of the core dielectric and those at the peaks indicate the positions of the metal slabs. The inset in Fig. 4(b) is the magnified H_z profiles around the 20 *nm*-thick metal embedded in between the core (n_1) and the cladding (n_3). All the mode profiles reveal necessarily exponential decay in the cladding and hyperbolic-cosine distribution in the core, but the ratio of the field amplitudes at the two metal-dielectric interfaces is quite different with each other. At D = 0.3 μm, before the transient saturation in propagation length, the field amplitude is smaller at the metal-core interface and it grows up inside the metal layer as approaching the metal-cladding interface. At D = 1.0 μm within the transient saturation region or at D = 4.0 μm after it, on the other hand, the field amplitude, decreases down toward the metal-cladding interface. This difference in the field profiles can be understood by a transition property of the mode profiles between two limiting cases of D = 0 and $D\rightarrow\infty$: When the core thickness shrinks to be zero the field profiles on two metal slabs combine together to make a single hyperbolic-cosine form, therefore the field amplitudes on both sides of the metal-dielectric interfaces become higher than that in the middle of the metal layer. If the core thickness is large enough not to allow any field coupling between the two metals, the field in each metal slab has a larger amplitude on the metal boundary facing the dielectric with a lower refractive index since the evanescent tail of the field profile is stretched further into the lower dielectric.

In case of the high-index core shown in Fig. 5, change in the propagation length as D varies is moderate with no drastic increase for all three wavelengths. (Note that the vertical scale is linear, not logaritmic as in Fig. 4(a)). For λ_0 = 1550 *nm* the propagation length decreases gradually down to a minimum at D = 3 μm before its increase. The normalized H_z profiles for D = 0.3, 3.0, and 8.0 μm depicted in Fig. 5(b) imply that the energy portion localized in the core region becomes larger as increasing D and the mode approaches to a fundamental mode of dielectric slab waveguides. Also, the field amplitudes inside the metal

#89161 - $15.00 USD Received 29 Oct 2007; revised 29 Nov 2007; accepted 29 Nov 2007; published 7 Dec 2007

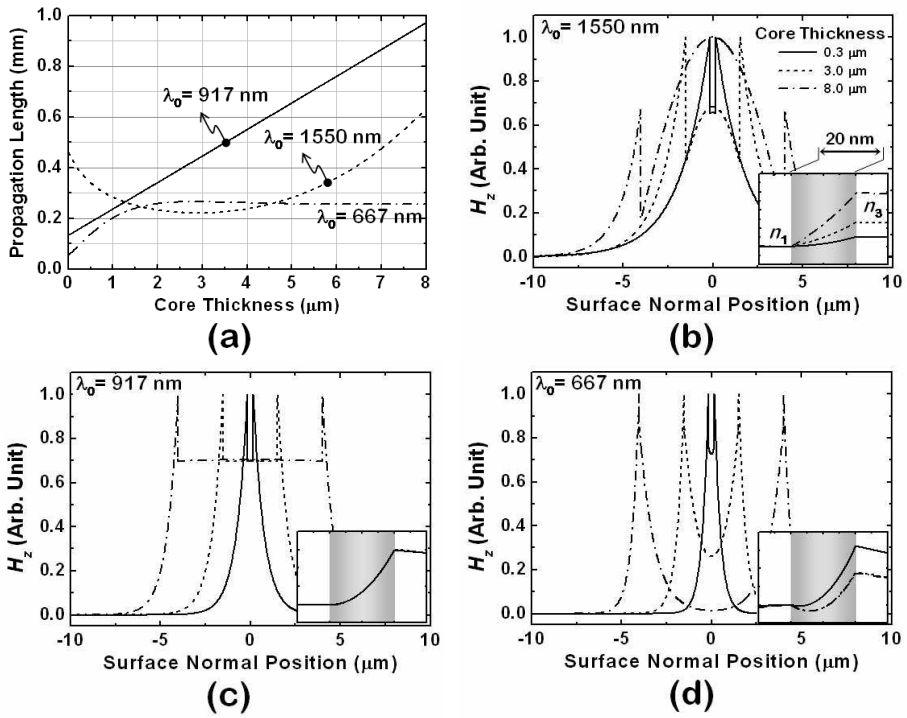

Fig. 5. (a). Dependences of the propagation lengths of sc-LRSPPs on the core thickness for the case of high index core at several wavelengths. The vacuum wavelengths are selected as representatives for $\omega<\omega_c$ (dotted line), $\omega=\omega_c$ (solid line) and $\omega>\omega_c$ (dash-dotted line). Please note that, differently from Fig. 4(a), the vertical axis is not logarithmic but linear scale. (b), (c), and (d) shows the field profiles (H_z) of sc-LRSPPs for several core thicknesses at $\omega<\omega_c$, $\omega=\omega_c$, and $\omega>\omega_c$ respectively. The inset in each figure shows the profiles normalized by its value at the core-metal interface in the metal film (grey region).

layer always grow up as approaching the metal-cladding interface as shown in the inset of Fig. 5(b).

For $\lambda_0 = 917\ nm$ ($\omega = \omega_c$), dependence of the propagation length on D and evolution of the field profiles are quite interesting as depicted in Figs. 5(a) and 5(c), respectively. The propagation length is linearly proportional to D. Regardless of the core thickness, the field amplitude is uniform over the whole core region and the normalized field profiles around the metal layers are exactly matched with each other as shown in the inset of Fig. 5(c). These distinctive characteristics at $\omega = \omega_c$ are caused by the fact that $\beta = n_1 k_0$ thus $\alpha_1 = 0$ for arbitrary core thickness. The non-dispersive property of the propagation constants on D also insists that α_2 and α_3 must be constant, therefore, not only the decay lengths to the core and cladding dielectrics but also the amplitudes of the exponents given in Eq. (5) should be constant. It must be emphasized that this particular property is very desirable for adiabatic coupling between optical modes with different lateral sizes via waveguide tapering. Adiabatic coupling is reasonable under the condition that the eikonal parameter defined by $\tan(\phi)[d(1/\beta_r)/dD]$ should be much less than 1, where ϕ is a taper angle [29]. The eikonal parameter is zero for sc-LRSPP modes with the characteristic frequency, resulting that a very large tapering angle can be acceptable for an efficient mode coupling. Moreover, the flat-top profiles of the field amplitudes in the core are sustained even for a large core-thickness variation. This may offer a noble method for flat-top beam shaping of light radiated from a conventional waveguide or a point-like source.

#89161 - $15.00 USD Received 29 Oct 2007; revised 29 Nov 2007; accepted 29 Nov 2007; published 7 Dec 2007

Finally over a higher frequency range of $\omega > \omega_c$, core-thickness dependence of the propagation length in Fig. 5(a) and the mode profiles in Fig. 5(d) are not so different from those of the low-index-core case. The modes converge to a decoupled LRSPP mode from a sc-LRSPP as increasing D with no distinct feature in between.

It may be worth considering whether such a crossing in dispersion curves as shown in Fig. 2(b) also takes place in a two dimensional guiding structure, like a cylindrical plasmonic waveguide consisting of a metal coated high-index dielectric wire surrounded by a low-index cladding [30]. Actually the SPP mode represented by n = 1 in a higher branch of dispersion curve of the cylindrical plasmonic waveguide, where n is the number of azimuthal oscillation, also has a crossing point near the core light line. According to Ref. 30, dispersion curves for higher branch of n = 1 modes cross core light line and curves for different core diameter intersect with each other. Therefore, it can be concluded that there exists flat-top modes (α_1 = 0) and nearly non-dispersive characteristics on core diameter. But unfortunately, we have found that the crossing point does not always correspond to the core light line after an intuitive consideration as follow: Noted that one of the physical origins of the non-dispersive characteristic at $\omega = \omega_c$ results from the separable property of the exponential functions in Eqs. (4) and (5) so as to satisfy $\exp[\pm\alpha_2(D+t)] = \exp(\pm\alpha_2 D)\exp(\pm\alpha_2 t)$. These separable functions guarantee to eliminate the term $\exp(\pm\alpha_2 D)$ in Eqs. (4) and (5), and only the exponents having $\pm\alpha_1 D$ argument among the D dependent terms survive before they disappears when $\alpha_1 = 0$ at $\omega = \omega_c$. However, such elimination is not possible in a cylindrical plasmonic waveguide because its mode expression does not consist of exponential functions any more but modified Bessel functions of second kind. Therefore, a flat-top mode exists in a cylindrical plasmonic waveguide, but it does not always have non-dispersive characteristic on core diameter. Though the two noble properties do not always coincide with each other, it will be interesting to find out other 2-dimensional structures that support efficient flat-top collimation or coupling between optical source and μm-scale waveguide.

6. Conclusion

For double-electrode plasmonic waveguide structures, modal properties of the sc-LRSPPs have been described comprehensively by investigating frequency dependence of the dispersion relation and the mode profiles consistently. We have found out that the sc-LRSPP modes excited on a double-electrode plasmonic waveguide can be classified by four groups of distinctive characters according to their dependence on the core thickness D. For the low-index-core structure, the propagation length can be largely extended at a particular core thickness of wavelength scale at a frequency range lower than the characteristic frequency ω_c which depends on the index difference in the core-cladding layers and the thickness of the metal. The characteristic of drastic increase in the propagation length may be used not only for refractrometric sensors or non-linear ATR devices but also variable optical attenuators by incorporating media for active index modulation as a core dielectric [19]. For a frequency range higher than ω_c, the sc-LRSPP mode converts its modal property moderately from symmetrically coupled to decoupled as D increases. For the high-index-core structure, on the other hand, there is no cut-off core thickness in overall frequency range. For $\omega < \omega_c$ the sc-LRSPPs with a large D converge to a mode of conventional dielectric slab waveguides, but at $\omega = \omega_c$ the sc-LRSPP modes are completely non-dispersive for change in D. Regardless of D alteration, the modes at $\omega = \omega_c$ consistently maintain a perfect flat-top profile in the core region and identical decay tails in the cladding. 2-dimensional extension of this prominent characteristic may provide us a novel means for uniform dimension-scaling and flat-top profile-shaping of an optical mode tightly guided by plasmonic waveguides. Thus it will be worth to find out conditions for flat-top modes in a cylindrical waveguide with metal coated dielectric core. The flat-top sc-LRSPP modes may excite an active medium sandwiched in

#89161 - $15.00 USD Received 29 Oct 2007; revised 29 Nov 2007; accepted 29 Nov 2007; published 7 Dec 2007

between the metal layers very uniformly, therefore it will be interesting to implement such a non-dispersive flat-top mode for nonlinear applications of SPP waveguides.

Acknowledgments

This work was supported by an ETRI (Electronics and Telecommunications Research Institute) of Korea committed project (Grant No. 1010-2006-0111).

#89161 - $15.00 USD Received 29 Oct 2007; revised 29 Nov 2007; accepted 29 Nov 2007; published 7 Dec 2007